




Power Cycling Reliability with Temperature Deviation of Pressureless Silver Sintered Joint for Silicon Carbide Power Module

WON SIK HONG ^{1,2} and MI SONG KIM¹

1.—Electronic Convergence Materials and Device Research Center, Korea Electronics Technology Institute (KETI), #25, Saenari-ro, Bundang-gu, Seongnam-si, Gyeonggi-do 13509, Republic of Korea.
2.—e-mail: wshong@keti.re.kr

SiC devices can enhance power conversion in electric vehicles. However, traditional soldering techniques are limited by their low melting temperatures. Therefore, we used pressureless Ag sintering to assemble a 1200 V/200 A SiC metal-oxide-semiconductor field-effect transistor power module and compared the long-term reliability, electrical properties, and driving performance of the module with those of a similar module assembled using the solder Sn-3.0Ag-0.5Cu (SAC305). To assess sinter joint reliability, we performed power cycling tests over two temperature ranges, 50–150°C and 50–175°C, for 15,000 cycles. Subsequently, we compared the breakdown voltage (BV_{DSS}) and drain-source on-resistance ($R_{DS(ON)}$) of the SiC power modules and performed cross-sectional analyses of the device bonding interfaces. No difference in BV_{DSS} was found between the Ag-sintered and SAC305-soldered joints. However, the $R_{DS(ON)}$ exhibited minimal variation for the Ag-sintered module but significantly varied for the SAC305-soldered module, suggesting that the former better maintained its characteristics. Furthermore, the electrical characteristics of the SAC305-soldered module underwent more significant alterations with increasing temperature change during power cycling, indicating that cracks propagated throughout the SAC305 soldered joint over time. Therefore, Ag sintering was quantitatively validated as the superior die attachment technology compared to soldering for long-term reliability.

INTRODUCTION

The surge in electric vehicle (EV) usage has precipitated a corresponding rise in the demand for power modules, which are pivotal for vehicle power conversion. To enhance power conversion efficiency, manufacturers are innovating various module packaging structures, including the adoption of double-sided cooling packages within traditional case-type structures to optimize cooling efficacy. There are two types of performance enhancement strategies: (1) structural and design modifications and (2) the integration of SiC devices into Si-based power modules,^{1–9} with the latter

being an ongoing development. SiC devices exhibit high efficiency, output, voltage, and current capabilities that are superior to traditional Si devices.^{1–5} Power SiC MOSFET devices are mostly used for switching, so they are used to reduce on-voltage (on-resistance) and speed-up switching. Power MOSFETs are ideal power control devices because of their high speed and high breakdown voltage. Recently, the use of SiC WBG devices has been increasing because their switching performance is significantly superior to that of currently used Si. Furthermore, wide bandgap (WBG) devices such as GaN power modules afford high-speed switching but are limited to operating in a power range of approximately 600–800 V. Consequently, for EV applications necessitating power modules of ≥ 1200 V/200 A,^{4–14} SiC devices are indispensable. However, SiC devices, which exhibit maximum

(Received November 11, 2023; accepted January 17, 2024;
published online February 8, 2024)

junction temperatures of only up to 300°C during operation,⁹ preclude traditional soldering techniques owing to the risk of remelting. Therefore, a bonding technology that is impervious to high operational temperatures is necessary. Hence, Ag sinter bonding technology, which remains stable up to the melting point of Ag at 960°C, is actively being researched. However, despite active advancements in alternative Ag sintering bonding processes^{2,4–14} and materials,^{2–18} a comprehensive comparison detailing the performance and long-term reliability differences between soldered and sintered modules has not yet been accurately delineated.

Generally, thermal cycle testing and power cycle testing are used as test methods to verify the long-term reliability of power modules.^{2,5,6,8} Thermal cycle testing is a method of verifying the reliability of power modules due to differences in thermal expansion coefficient according to temperature changes between high and low temperatures. It is mainly used to verify the reliability of the bonding interface between a base plate and a ceramic substrate with a large bonding area. The power cycle test is a test method to verify whether thermo-mechanical fatigue cracks occur at the bonding interface of the MOSFET device because of heat generated while the device is operating. Therefore, in this study, a reliability evaluation was conducted using a power cycle test to verify the reliability of the module according to the MOSFET joining method.

Therefore, to evaluate the electrical characteristics and joint reliability, we developed 1200 V/200 A SiC MOSFET power modules for EVs utilizing pressureless Ag-sintered interconnections at 220–240°C and Sn-3.0Ag-0.5Cu (SAC305) soldering at 245°C. The soldered and Ag-sintered joints were compared by conducting two distinct power cycling tests (PCTs). In addition, we measured and compared the drain-source on-resistance ($R_{DS(ON)}$) and breakdown voltage (BV_{DSS}) of the SiC MOSFET power modules before and after the PCTs. To ascertain the quality of the Ag sintered joints, we conducted assessments of the bonding layer thickness (BLT), densification, void content, and shear strength using X-ray non-destructive microscopy, scanning electron microscopy (SEM), energy dispersive X-ray spectroscopy (EDS), and cross-sectional analysis techniques.

EXPERIMENTAL PROCEDURES

Raw Materials and Pressureless Ag-Sintering and Soldering Process

Sn-3.0Ag-0.5Cu (SAC305) solder paste (LFSOLDER TLF-204-HSP, Tamura Chemical Co. Ltd., Japan) and Ag paste (CT2700R7S, Kyocera Chemical Co., Japan, containing 90 wt% Ag powder) were used for vacuum soldering and pressureless Ag sintering to assemble SiC MOSFET power modules. Figure 1a, b, and c shows photographs of the Ag

paste printed on a Si_3N_4 active metal-brazed (AMB) substrate with an Ag finish on a Cu layer, with a width of 30.0 mm, length of 37.5 mm, and thickness of 920 μm (0.3 (Cu)/0.32 (Si_3N_4)/0.3 (Cu) mm). A 1200 V/200A and 25 $\text{m}\Omega$ live SiC MOSFET device (CPM2-1200-0040B, Cree Co., USA) was then mounted on the Ag paste-printed substrate. The base-plate material of the MOSFET device was a C1120 copper (90.0 mm \times 45.0 mm \times 3.0 mm) plate with 5 μm Ni plating. Figure 1c shows the pressureless Ag sintering process in a vacuum reflow system (RSS-210-S, UniTemp GmbH, Germany). Figure 1d shows a temperature and pressure profile for the pressureless vacuum Ag sintering process.

To compare the electrical properties and joint reliability performance of Ag-sintered and soldered joints in SiC power modules, the same type of SiC power module was prepared with the SAC305 soldered using a vacuum soldering machine (VSD-3030, Shinko Seiky Co., Ltd., Japan). The temperature and time of preheating, peak temperature, and reflow soldering time were 150–180°C, 166 s, 240°C, and 136 s, respectively.

Also, the densification of Ag-sintered joints was measured. The cross-sectional morphologies and porosities of the Ag-sintered joints were examined. The densification of the Ag-sintered joint, which was calculated as the ratio of the porosity to the sintered joint area, was determined using the *i*-Solution software (Image & Microscope Technology Inc., USA).

Breakdown Voltage (BV_{DSS}) and Drain-Source On-Resistance ($R_{DS(ON)}$) Measurement of SiC MOSFET Power Module Before and After Power Cycling Test

To measure the electrical properties of the SiC power module, the BV_{DSS} and $R_{DS(ON)}$ between the source area of the MOSFET top surface and the bonding drain of the substrate were measured. Thus, the resistance value changes according to the interconnection method of the SiC MOSFET device bonding.

BV_{DSS} between source-drain is usually determined more by the chip than the joint, which is located outside of the chip, unless the voltage is affected by an increase in joint resistance. However, to compare the difference in electrical characteristics between the solder joint and the sintered joint, the BV_{DSS} and $R_{DS(ON)}$ can be performed simultaneously to determine whether damage has occurred in the MOSFET joint.

The electrical properties were measured using a power device analyzer for circuit design (Keysight B1506A) and a switching tester (WT1800, Yokogawa Co., Japan). The fundamental electrical properties were assessed using the double-pulse test method under 600 V and 200 A conditions, with the gate resistance set at 10 Ω and inductance at 40 μH .

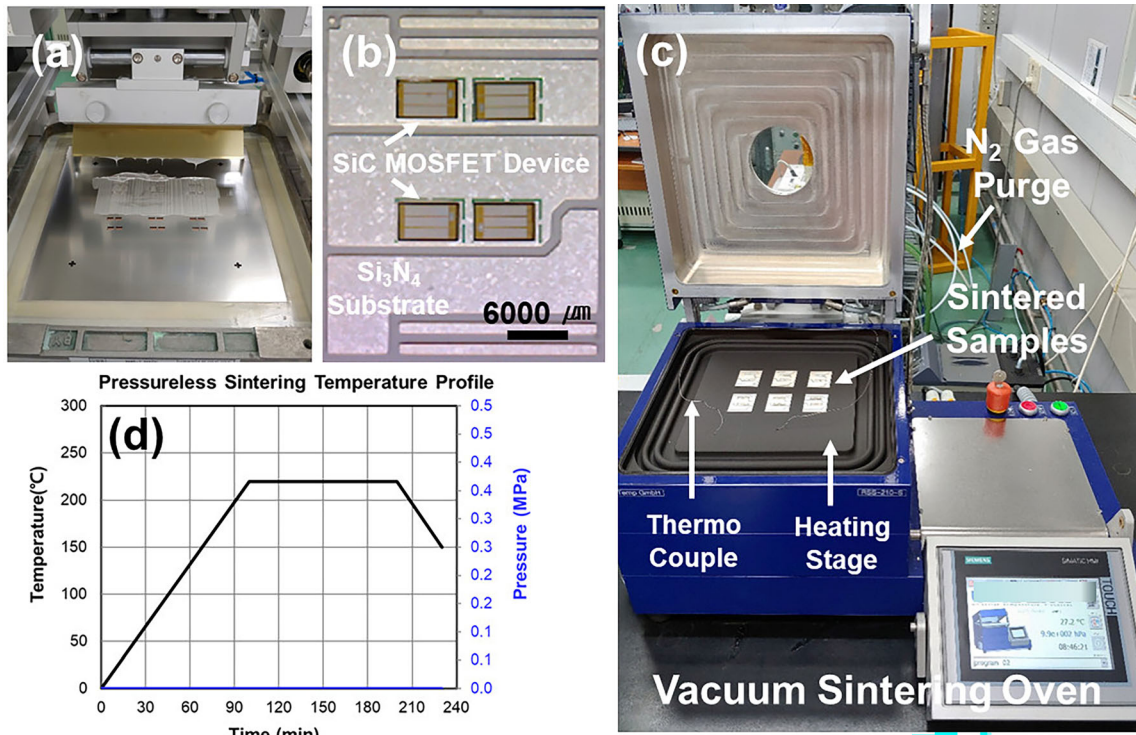


Fig. 1. Photographs of (a) Ag paste printing process, (b) SiC device mounted on the Si₃N₄ AMB substrate, and (c) sintering samples in the vacuum sintering oven. (d) Temperature and pressure profile for Ag sintering.

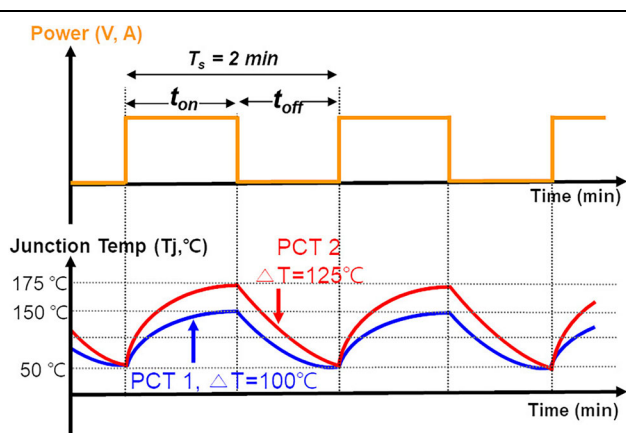


Fig. 2. Power and junction temperature profile of temperature deviation (ΔT) of PCT 1 and PCT 2 conditions during power cycling.

Both sintered and soldered modules underwent testing with identical gate drivers to determine whether disparities in BV_{DSS} and $R_{DS(ON)}$ existed. An increase in $R_{DS(ON)}$ would indicate the presence of cracks at the joint interface or variations in the bonding materials. Hence, $R_{DS(ON)}$ served as the preferred metric for comparing the characteristics of the bonding layers.

To compare the electrical properties and reliability performance, the Ag-sintered and SAC305 soldered joints of the 1200 V/200 A SiC MOSFET power modules were tested using PCT under two temperature conditions (Fig. 2): PCT 1 under a

temperature range of 50–150°C ($\Delta T = 100^\circ\text{C}$) and PCT 2 under 50–175°C ($\Delta T = 125^\circ\text{C}$), for 15,000 cycles each. Figure 2 shows the temperature deviations of PCT 1 and 2 as well as the power and junction temperature profiles during the PCTs. The BV_{DSS} and $R_{DS(ON)}$ of the power modules were measured and compared before and after the tests.

RESULTS AND DISCUSSION

Shear Strength and Void Content of Pressureless Ag-Sintered SiC Chip and Si₃N₄ AMB Substrate Joints and MOFET Module Assembly

Figure 3a, b, and c shows the void content measurements for the pressureless Ag sintered joint comprising a SiC MOSFET device and Si₃N₄ AMB substrate, as obtained via X-ray non-destructive analysis. Post sintering, the void content within the pressureless Ag joint layer ranged from 0.7% to 2.6%, indicating exemplary joint formation. The corresponding shear strength ranged from 33.0 MPa to 48.0 MPa (Fig. 3c). Before employing live SiC MOSFET modules, we refined the sintering conditions using a dummy SiC chip that mirrored the geometry of the live die. Subsequent sintering processes on live SiC devices yielded shear strengths between 40.6 MPa and 42.5 MPa. According to previous research by Hong et al.⁵ solder joint integrity is maintained when the void content ranges from 0.4% to 2.4%, and the

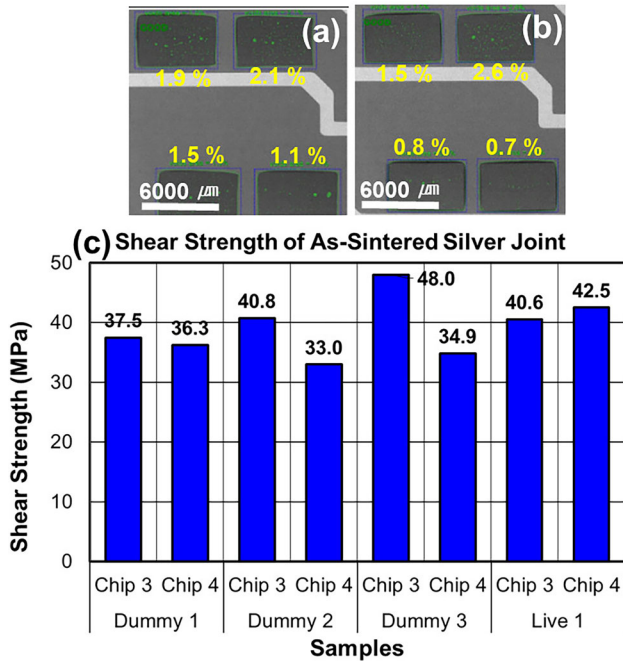


Fig. 3. (a, b) X-ray non-destructive analysis results of pressureless Ag-sintered module with SiC MOSFET and Si_3N_4 AMB substrate and (c) shear strength of Ag-sintered SiC MOSFET joints.

assembled power modules must exhibit a maximum of 3% voids at base-plate soldered joints while being devoid of cracks or delamination.⁵ Generally, there is no intermetallic compound at the joint interface of the Ag sinter joint, and it is found to be superior in terms of reliability because it has high joint strength and stability at high temperatures compared to solder.

The requisite strength of sintered joints is generally 25–80 MPa. Notably, if joint strength surpasses that of traditional soldered joints, the brittleness may increase, which can compromise the capacity of the power module to absorb stresses from warping or external forces. Therefore, maintaining an optimal joint strength is crucial for reliability. By these benchmarks, the bond strength observed in our study was maintained at a suitable level, aligning with the established standards for reliability.

A power module was fabricated to ascertain the electrical properties of the sintered joint and to conduct PCTs. The completion of power module assembly, preparatory to operation, entailed several stages: bonding wires for circuit connectivity, attaching terminals and signal pins, and assembling the case. Figure 4 provides a sequential visual narrative of the power module assembly following pressureless Ag sinter bonding. Specifically, Fig. 4a shows the module with a SiC MOSFET and Si_3N_4 AMB substrate post-sintering, Fig. 4b shows the addition of the base plate, Fig. 4c shows the module with aluminum wire bonds, power terminations, and signal pins in place, and Fig. 4d shows the fully

assembled power module encased in its final plastic housing.

$R_{\text{DS(ON)}}$ and E_{SW} of SiC MOSFET Power Modules Bonded with Sn-3.0Ag-0.5Cu Soldering and Ag Sintering

Figure 5 compares the electrical properties BV_{DSS} and $R_{\text{DS(ON)}}$ of the power modules before and after undergoing PCTs; Fig. 5a and b shows the PCT 1 conditions ($\Delta T_j = 100^\circ\text{C}$) and PCT 2 conditions ($\Delta T_j = 125^\circ\text{C}$), respectively. Under both PCT 1 and 2 conditions, following 15,000 cycles, the BV_{DSS} for both the Ag-sintered and SAC305 soldered joint modules remained steady at 1.61–1.67 kV, indicating stable insulation within the power module. However, a marked variance was observed in the $R_{\text{DS(ON)}}$ values of the sintered and soldered joint modules, contingent upon the PCT conditions. Notably, under the more stringent PCT 2 conditions, the $R_{\text{DS(ON)}}$ of the soldered joint module exhibited a significant rise. Prior to testing, the low and high side $R_{\text{DS(ON)}}$ for the sintered and soldered joint modules was 7.36/7.34 m Ω and 7.85/7.83 m Ω , respectively; post testing, these values shifted to 7.48/7.51 m Ω for the sintered joints and to 7.99/8.33 m Ω for the soldered joints. The initial lower $R_{\text{DS(ON)}}$ of the sintered joints compared to the soldered joints can be attributed to the superior thermal conductivity of Ag (419 W/m \cdot K) compared to that of SAC305 soldered (55 W/m \cdot K), which resulted in reduced thermal resistance and consequently $R_{\text{DS(ON)}}$ during module operation.^{4,5}

In contrast, for PCT 2, the initial low and high side $R_{\text{DS(ON)}}$ for the sintered and soldered joint modules was 7.29/7.37 m Ω and 7.68/7.64 m Ω , respectively. Post testing, $R_{\text{DS(ON)}}$ values of 7.34/7.5 m Ω for the sintered joints and 7.75/9.25 m Ω for the soldered joints were obtained, indicating a swift increase in the $R_{\text{DS(ON)}}$ for the soldered connections. This trend demonstrates that under harsh PCT conditions, the stability of Ag-sintered joints surpasses that of soldered joints. These findings confirm that soldering is unsuitable for bonding SiC devices, particularly under high junction temperature deviation (here, $\Delta T_j = 125^\circ\text{C}$).

Bonding Layer Thickness, Densification, and Microstructure of Pressureless Ag-Sintered and Sn-3.0Ag-0.5Cu Soldered SiC MOSFET Power Modules

Figure 6a and b shows the BLT and densification of the pressureless Ag sintered joints before and after undergoing the PCTs, with accompanying photographs documenting the densification measurement process of the pressureless Ag sintered joints. The data correlating to BLT and densification post-thermal cycling are referenced from a previous study by Hong et al.⁵ The BLT measurements before and after the PCT were 71.4 μm and 78.3 μm , respectively, with densification remaining nearly

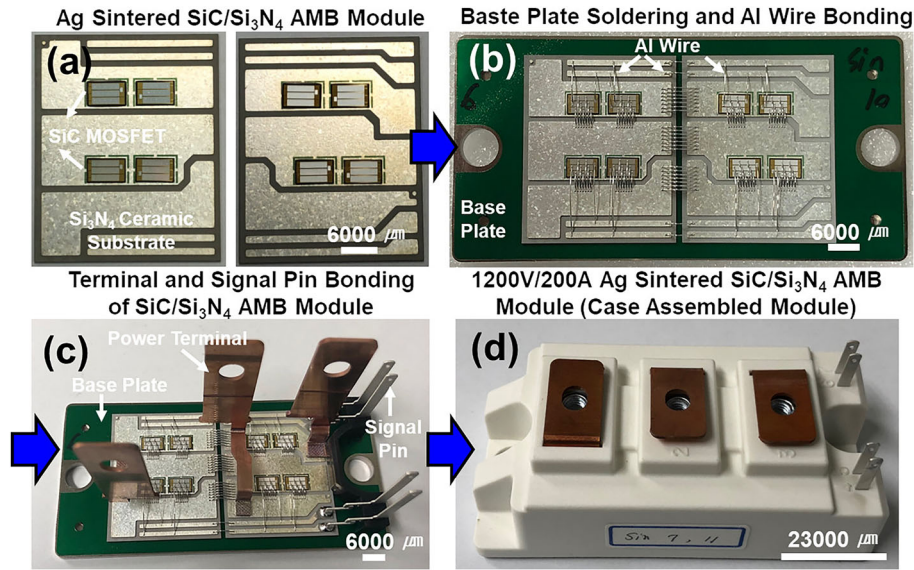


Fig. 4. Photographs of SiC MOSFET power module assembly procedure (a) after pressureless Ag sintering of SiC MOSFET and silicon nitride AMB substrate, (b) base-plate and aluminum wire bonding, (c) power termination and signal pin bonding, and (d) plastic case assembly.

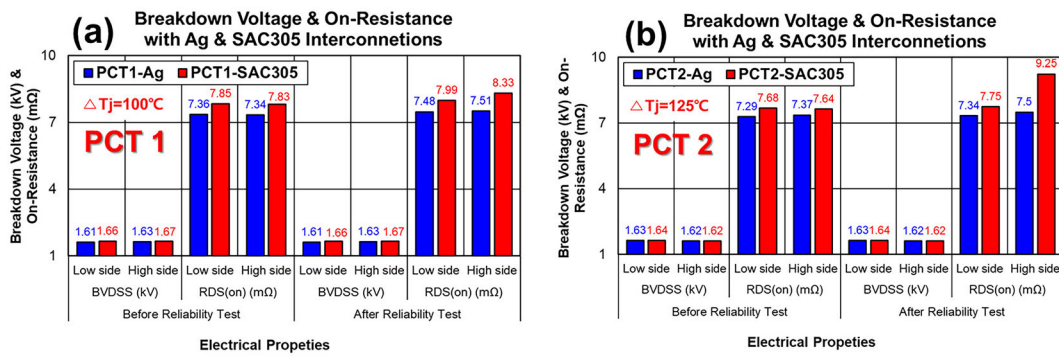


Fig. 5. Comparison between the BV_{DSS} and $R_{DS(ON)}$ values of the Ag-sintered and SAC305 soldered SiC MOSFET power modules before and after power cycling tests: (a) PCT 1 ($\Delta T_j = 100^\circ C$), (b) PCT 2 ($\Delta T_j = 125^\circ C$).

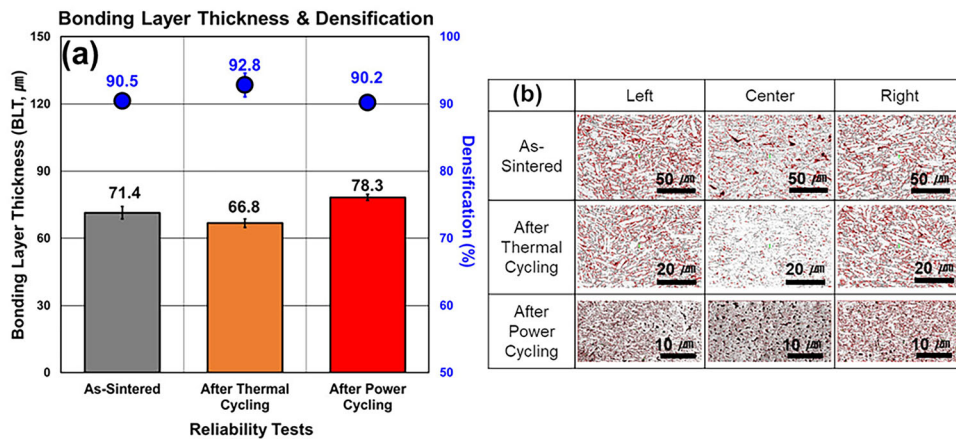


Fig. 6. (a) Comparison of bonding layer thickness and densification before and after thermal cycling⁵ and power cycling tests. (b) Photographs for measuring the densification of pressureless Ag sintered joints.

constant (90.5% and 90.2%, respectively). These metrics align with the findings from the prior study by Hong et al.,⁵ wherein BLT and densification after

thermal cycling were reported as 66.8 μm and 92.8%, respectively. For Ag sinter joint, the diffusion reaction in the Ag sinter layer continuously

occurred during the thermal and power cycling test. Therefore, the densification increased somewhat after PCT.^{5,6}

Figure 7a and b shows images of a pressureless Ag-sintered 1200 V/200 A SiC MOSFET power module before and after the PCT, respectively. Figure 7c shows the X-ray non-destructive analysis results of the Ag sintered joint. Figure 7d, e, f, g and h shows cross-sectional SEM micrographs of the pressureless Ag sintered joint. Figure 7i, j, k and l shows magnified images of the Ag sintered joint

interfaces on the SiC MOSFET and Si₃N₄ AMB substrate sides, as referenced in Fig. 7g. Post-PCT examinations confirmed the absence of voids and cracks within the pressureless Ag-sintered joints and evidenced the presence of well-maintained networks between Ag powders both within the sinter matrix and at the interfaces. This maintenance of microstructural integrity is posited as the reason for the negligible changes in BV_{DSS} and $R_{DS(ON)}$.

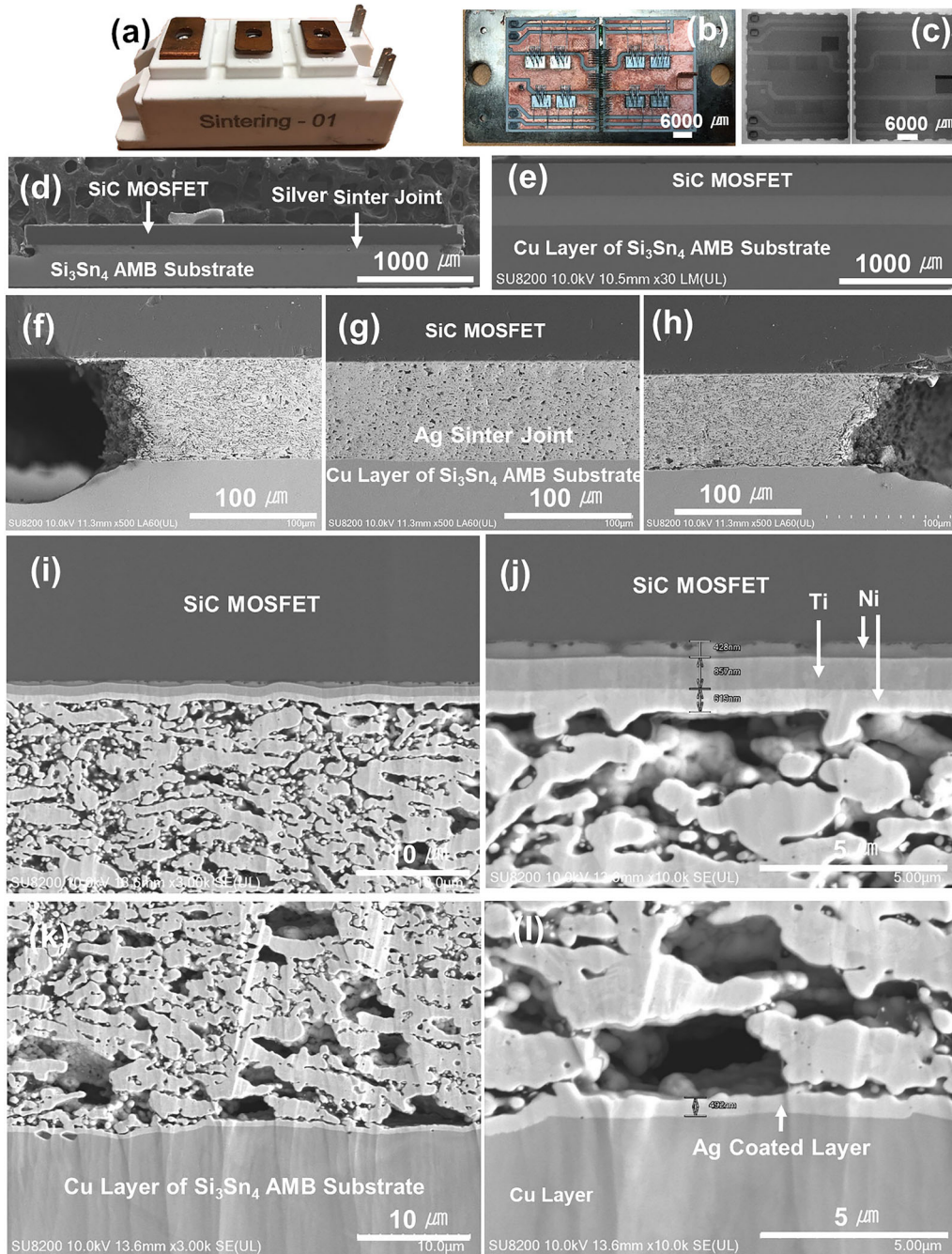


Fig. 7. (a, b) Photograph of 1200 V/200 A SiC MOSFET power module after power cycling test. (c) X-ray non-destructive analysis results of Ag sintered joint. (d–h) Cross-sectional SEM micrographs of pressureless Ag sintered joint. Magnified SEM images of (i, j) SiC MOSFET side and (k, l) Ag-coated Si₃N₄ AMB substrate side of Ag-sintered module.

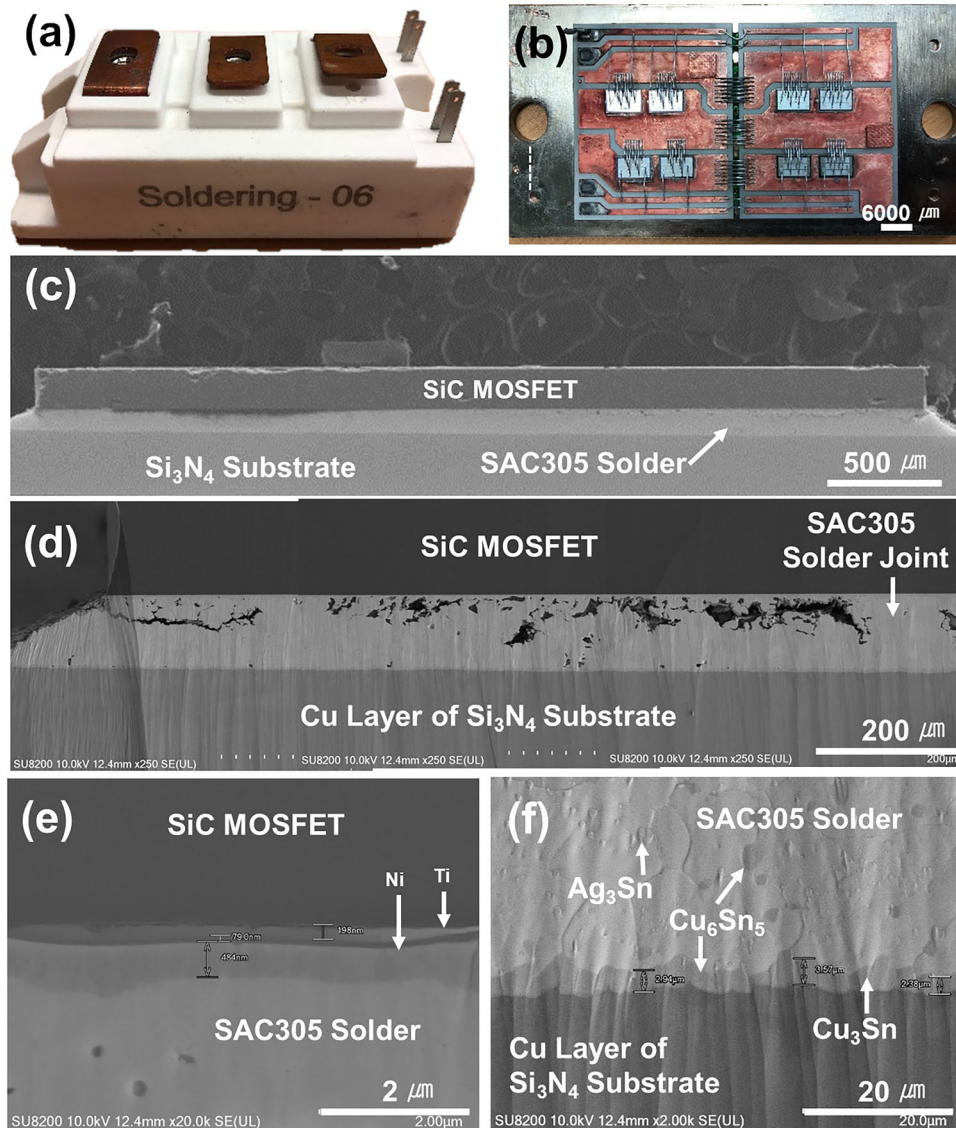


Fig. 8. (a, b) Photograph of 1200 V/200 A SiC MOSFET power module after power cycling test. (c, d) Cross-sectional SEM micrographs of Sn-3.0Ag-0.5Cu soldered joint. Magnified SEM images of (e) SiC MOSFET side and (f) Ag-coated Si₃N₄ AMB substrate side of soldered module.

Conversely, Fig. 8a and b shows a SAC305 soldered 1200 V/200 A SiC MOSFET power module after undergoing PCTs. Figure 8c and d shows cross-sectional SEM micrographs of the SAC305 soldered joint, while Fig. 8e and f shows magnified SEM views of the SiC MOSFET side and Ag-coated Si₃N₄ AMB substrate side, respectively. In stark contrast to the sintered joint, these images revealed crack propagation throughout the SiC MOSFET joint interface in the soldered joint module after 15,000 power cycles. This cracking contributed to the notable increases in BV_{DSS} and $R_{DS(ON)}$ post PCT. Consequently, these findings verify that solder bonding is unsuitable for die attachment in power modules that employ SiC semiconductors, and Ag sintering is more reliable.

Figure 9 shows the SEM images and EDS line profile of the pressureless Ag sintered joint (Fig. 9a,

b, c, and d) and SAC305 soldered joint (Fig. 9e, f, g and h) between the SiC MOSFET and Si₃N₄ AMB substrate. There was evidence of inter-diffusion between Ag and Ni within the Ag matrix and the Ni back metallization layer of the MOSFET device for the Ag sintered joint. Similarly, inter-diffusion between the Ag and Cu layers^{5,6,8,16-18} was observed on the AMB ceramic substrate side of the sintered joint. These inter-diffusions contribute to the formation of a networked structure within the Ag sinter layer during the sintering process,^{5,6,8} indicating that the integrity of the joint was established through inter-diffusion within the sintered matrix.

Meanwhile, the SAC305 soldered joint exhibited the formation of Cu₆Sn₅ and Ag₃Sn intermetallic compounds (IMCs) within the solder matrix. Specifically, a Cu₆Sn₅ IMC layer was identified at the soldered joint interface on the AMB substrate side.

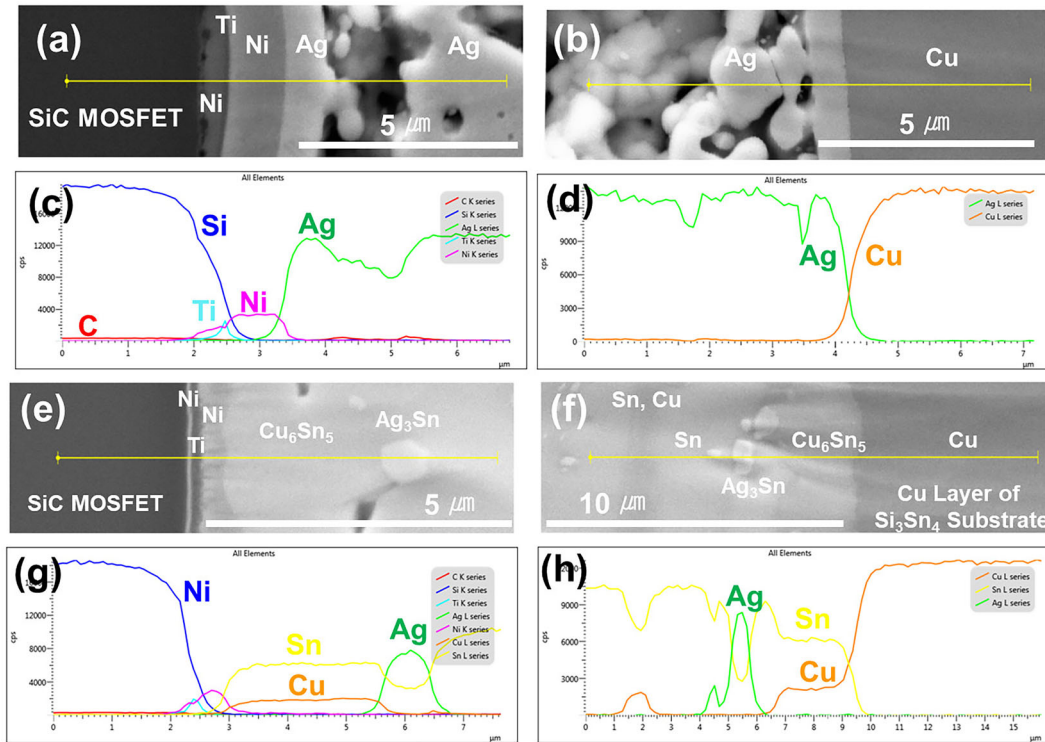


Fig. 9. SEM images of the joint interfaces of (a) Ag-sintered SiC MOSFET and (b) Si_3N_4 AMB substrate sides. EDS line profile analysis results of (c) Ag-sintered SiC MOSFET and (d) Si_3N_4 AMB substrate sides. SEM images of the SiC MOSFET soldered joints of (e) chip and (f) substrate sides. EDS line profile analysis results of (g) chip and (h) substrate sides.

The formation of these IMCs is typical in soldered joints and is known to enhance the initial joint strength.^{19–21}

CONCLUSION

In this study, we refined a pressureless Ag sintering process to affix a 1200 V/200 A SiC MOSFET device to a Si_3N_4 AMB substrate; the process was conducted at 220–240°C for 90 min under vacuum in a nitrogen atmosphere. The Ag sintered joint showcased a void content ranging over 0.7–2.6%, with the BLT before and after PCT recorded at 71.4 and 78.3 μm , respectively. The level of densification remained consistent, measured at 90.5% before and 90.2% after the PCT.

For comparative analysis of electrical properties and reliability, an identical module was also prepared using the SAC305 soldering process. By conducting two variations of PCT with different temperature conditions—PCT 1 (50–150°C, $\Delta T_j = 100^\circ\text{C}$) and PCT 2 (50–175°C, $\Delta T_j = 125^\circ\text{C}$)—for 15,000 cycles, we assessed and compared the BV_{DS} and $R_{\text{DS(ON)}}$ of the power modules before and after the PCTs. During PCT 1, the sintered module exhibited minimal change in $R_{\text{DS(ON)}}$ under the ΔT_j of 100°C; however, the soldered module showed an increase in $R_{\text{DS(ON)}}$ from 7.83/7.85 m Ω to 8.33/7.99 m Ω . During PCT 2, when subjected to the greater temperature deviation of $\Delta T_j = 125^\circ\text{C}$, the $R_{\text{DS(ON)}}$ of the soldered module increased

significantly (7.68/7.64 m Ω to 7.75/9.25 m Ω), in stark contrast to the sintered module (7.29/7.37 m Ω to 7.34/7.5 m Ω). This significant rise in $R_{\text{DS(ON)}}$ for the soldered module was attributed to crack formation at the soldered joints of the SiC MOSFET device. In comparison, the sintered module demonstrated a negligible increase in $R_{\text{DS(ON)}}$, exhibiting preserved stability of the bonding interface post PCT.

These findings therefore suggest that Ag sinter bonding is more stable and beneficial than soldering for attaching SiC devices in power modules, particularly for EV applications.

ACKNOWLEDGEMENTS

We thank Director Yongjin Joo of iA Powertron, Inc. (Incheon 21314, Republic of Korea) for helping with the assembly and electrical property measurements of the power modules.

CONFLICT OF INTEREST

The authors declare that they have no conflict of interest.

OPEN ACCESS

This article is licensed under a Creative Commons Attribution 4.0 International License, which permits use, sharing, adaptation, distribution and reproduction in any medium or format, as long as

you give appropriate credit to the original author(s) and the source, provide a link to the Creative Commons licence, and indicate if changes were made. The images or other third party material in this article are included in the article's Creative Commons licence, unless indicated otherwise in a credit line to the material. If material is not included in the article's Creative Commons licence and your intended use is not permitted by statutory regulation or exceeds the permitted use, you will need to obtain permission directly from the copyright holder. To view a copy of this licence, visit <http://creativecommons.org/licenses/by/4.0/>.

REFERENCES

1. T. Kunimune, M. Kuramoto, S. Ogawa, T. Sugahara, S. Nagao, and K. Sukanuma, *Acta Mater.* 89, 133 (2015).
2. H. Chin, K. Cheong, and A. Ismail, *Metall. Mater. Trans. B* 41, 824 <https://doi.org/10.1007/s11663-010-9365-5> (2010).
3. W.S. Hong, M.S. Kim, D. Kim, and C. Oh, *J. Electron. Mater.* 48(1), 122 <https://doi.org/10.1007/s11664-018-6769-5> (2019).
4. H. Lin, *Power SiC 2017: Materials, Devices and Applications* (France: Yole Development, 2017), pp.46–108.
5. W.S. Hong, M.S. Kim, and K.-K. Hong, *J. Electron. Mater.* 50(3), 914 <https://doi.org/10.1007/s11664-020-08698-3> (2021).
6. W.S. Hong, M.S. Kim, and C. Oh, *J. Electron. Mater.* 49(1), 188 <https://doi.org/10.1007/s11664-019-07654-0> (2020).
7. M. Abtew, and G. Selvaduray, *Mater. Sci. Eng. R. Rep.* 27, 95 [https://doi.org/10.1016/S0927-796X\(00\)00010-3](https://doi.org/10.1016/S0927-796X(00)00010-3) (2000).
8. W.S. Hong, M.S. Kim, C. Oh, Y. Joo, Y. Kim, and K.-K. Hong, *JOM* 72(2), 889 <https://doi.org/10.1007/s11837-019-03815-y> (2020).
9. K. Sheng, *IEEE Trans. Electron Devices* 56(2), 337 <https://doi.org/10.1109/TED.2008.2010605> (2009).
10. Y. Gao, A. Huang, S. Krishnaswami, J. Richmond, and A. Agarwal, *IEEE Trans. Ind. Appl.* 44, 887 <https://doi.org/10.1109/TIA.2008.921408> (2008).
11. S. Noh, H. Zhang, and K. Sukanuma, *Materials* 11, 2531 <https://doi.org/10.3390/ma11122531> (2018).
12. H. Zhang, C. Chen, S. Nagao, and K. Sukanuma, *J. Electron. Mater.* 46(2), 1055 <https://doi.org/10.1007/s11664-016-5069-1> (2017).
13. S.W. Yoon, M.D. Glover, and K. Shiozaki, *IEEE Trans. Power Electron.* 28(5), 2448 <https://doi.org/10.1109/TPEL.2012.2212211> (2013).
14. R.K. Williams, R.A. Blanchard, P. Rutter, and Y. Kawaguchi, *IEEE Trans. Electron Devices* 64(3), 692 <https://doi.org/10.1109/TED.2017.2655149> (2017).
15. J.S. Hirschhorn, *Introduction to Powder Metallurgy* (The Colonial Press Inc., USA, 1969), pp.155–273.
16. Y.-J. Lee, and J.-H. Lee, *Electron. Mater. Lett.* 18(1), 94 (2021).
17. E.B. Choi, Y.-J. Lee, and J.-H. Lee, *J. Alloys Compd.* 897(15), 163223 (2022).
18. Y.-J. Lee, and J.-H. Lee, *Met. Mater. Int.* 29, 1775 <https://doi.org/10.1007/s12540-022-01320-7> (2023).
19. W.S. Hong, C. Oh, M.S. Kim, Y.W. Lee, H.J. Kim, S.J. Hong, and J.T. Moon, *J. Electron. Mater.* 45(12), 6150 <https://doi.org/10.1007/s11664-016-4837-2> (2016).
20. W.S. Hong, and C.M. Oh, *J. KWJS* 31(3), 22 (2013).
21. W.S. Hong, and A.Y. Kim, *Mater. Trans. JIM* 56, 1002 <https://doi.org/10.2320/matertrans.MI201420> (2015).

Publisher's Note Springer Nature remains neutral with regard to jurisdictional claims in published maps and institutional affiliations.